International Journal of Quantum Information
Vol. 23, No. 5 (2025) 2550004 (20 pages)

DOI: 10.1142/S0219749925500042

Isospectral oscillators as a resource for quantum information processing

Abdelatif Chabane, Sidali Mohammdi and Abdelhakim Gharbi
Universite de Bejaia, Faculté des Sciences Exactes,
Laboratoire de Physique Théorique, 06000 Bejaia, Algérie

Matteo G. A. Paris*
Dipartimento di Fisica "Aldo Pontremoli",
Università degli Studi di Milano, I-20133 Milano, Italy
matteo.paris@fisica.unimi.it

Received 13 January 2025
Accepted 29 January 2025
Published 18 March 2025

In this paper, we address quantum systems isospectral to the harmonic oscillator, as those found within the framework of supersymmetric quantum mechanics, as potential resources for continuous variable quantum information. These deformed oscillator potentials share the equally spaced energy levels of the shifted harmonic oscillator but differ significantly in that they are nonharmonic. Consequently, their ground states and thermal equilibrium states are no longer Gaussian and exhibit nonclassical properties. We quantify their non-Gaussianity and evaluate their nonclassicality using various measures, including quadrature squeezing, photon number squeezing, Wigner function negativity, and quadrature coherence scale. Additionally, we employ quantum estimation theory to identify optimal measurement strategies and establish ultimate precision bounds for inferring the deformation parameter. Our findings prove that quantum systems isospectral to the harmonic oscillator may represent promising platforms for quantum information with continuous variables. In turn, non-Gaussian and nonclassical stationary states may be obtained and these features persist at nonzero temperature.

Keywords: Continuous variable quantum information; supersymmetric quantum mechanics; isospectral harmonic oscillators; non-Gaussianity; nonclassicality; quantum fisher information; ground states; thermal states.

1. Introduction

In quantum information processing, the unique features of continuous variable (CV) quantum systems make them valuable for certain tasks.[1–13] In particular, CV systems may be more robust against certain types of noise and de-coherence compared to discrete variable (DV) systems.[14,15] Additionally, CV systems, especially those

*Corresponding author.

realized on optical platforms, are experimentally accessible and can be implemented with existing technology. Finally, CV quantum computing involves fault tolerance[16] and error correction strategies[17] that differ from those used in DV systems and may be less expensive in terms of resources.

In CV quantum information, Gaussian states play an important role for their practical advantages, including simplicity in generation, detection, and manipulation. However, Gaussian states have a positive Wigner function,[18,19] making them of little use in several tasks including quantum simulations[20] and computation.[21] To overcome these limitations, non-Gaussian states have been widely investigated[22–28] and it has been shown that they can offer advantages and open up new possibilities in several tasks in quantum information science. In turn, non-Gaussian states often exhibit more pronounced nonclassical features compared to Gaussian states, thus providing more effective quantum resource for quantum teleportation,[25,29] quantum key distribution,[30–34] and quantum computation,[8,35–39] being also relevant for the detection of gravitational waves.[40–43] Those quantum non-Gaussian states are more challenging to generate, manipulate, and detect experimentally compared to Gaussian states, as their generation generally involves nonlinearity, conditional measurements, or quantum state engineering operations,[8,44,45] as for example, adding/subtracting photons,[24,46–50] which can induce and enhance the amount of nonclassicality (nonC) in an arbitrary quantum state.[51,52]

In this scenario, it would be extremely convenient to have a cheaper source of simultaneously non-Gaussian/nonclassical states to exploit their properties for CV quantum information processing without dealing with nonlinear processes, ancillary systems, and specialized detection methods. This is precisely the scope of this paper.

By using tools from supersymmetric quantum mechanics (SUSYQM), we consider systems described by deformed oscillator potentials, however strictly isospectral to the shifted harmonic oscillator (SHO).[53–58] This fact makes them suitable candidates for CV quantum information, since the potentials are not harmonic, and the ground states, as well as states in thermal equilibrium, are no longer Gaussian and exhibit nonclassical properties. Motivated by these facts, we set ourselves the task to investigate these states by quantifying their non-Gaussianity (nonG) through quantum relative entropy, and their nonC using quadrature squeezing, photon number squeezing, quadrature coherence scale (QCS) and Wigner function negativity. Finally, we address the characterization of isospectral SHO potentials, and seek for the optimal strategy to infer the deformation parameter, using tools from local quantum estimation theory (QET).[59–62] In this procedure, the figure of merit is the so-called quantum Fisher information (QFI), which provides a quantitative measure of the information about a parameter, which may be extracted by measurements performed on a family of quantum states.

This paper is structured as follows. In Sec. 2, we briefly provide an introduction to isospectral potentials in one-dimensional SUSYQM and report the properties of nonG and nonC as well as the possible measures to quantify these quantum resources, also review the ideas and the methods of local QET. In Sec. 3, we give the family of isospectral potentials for the SHO with its eigenfunctions spectrum. In Sec. 4, we address the use of nonG and nonC measures by taking into account two different families of stationary states, ground and thermal states, relevant to SHO isospectral potentials. In Sec. 5, we evaluate the QFI for the chosen states in order to infer the deformation parameter characterizing the SHO isospectral potentials, then we discuss results. Section 6 closes the paper by some concluding remarks.

2. Preliminaries

In this section, we review the main tools used in this paper: the notion of isospectral potentials in SUSYQM, the quantification of nonG and nonC, and finally the formalism of quantum estimation.

2.1. *Isospectral potentials in SUSYQM*

The formalism of supersymmetry allows for the construction, given some potential $V(x)$, of a family of potentials that have the same spectrum, and the same reflection and transition coefficients as the initial potential. In what follows we briefly review the method to generate a one-parameter isospectral family for a given potential. The ground state energy of the Hamiltonian need to be zero in order for the SUSYQM formalism to hold, this can be achieved without affecting the physics of the system by shifting the potential of the Hamiltonian. Let us first introduce the partner potentials $V^{(1)}(x)$ and $V^{(2)}(x)$ in terms of the superpotential $W(x)$

$$V^{(1)}(x) = W^2(x) - \frac{\hbar}{\sqrt{2m}} W'(x), \tag{1}$$

$$V^{(2)}(x) = W^2(x) + \frac{h}{\sqrt{2m}} W'(x). \tag{2}$$

One can factorize the Hamiltonian in two different ways by introducing the operators A and $A^\dagger$

$$A = \frac{\hbar}{\sqrt{2m}} \frac{d}{dx} + W(x), \tag{3}$$

$$A^\dagger = -\frac{\hbar}{\sqrt{2m}} \frac{d}{dx} + W(x). \tag{4}$$

We then write the corresponding partner Hamiltonians

$$H^{(1)} = A^\dagger A = -\frac{\hbar^2}{2m} \frac{d^2}{dx^2} + V^{(1)}(x),$$

$$H^{(2)} = A A^\dagger = -\frac{h^2}{2m} \frac{d^2}{dx^2} + V^{(2)}(x).$$

It is well established, when supersymmetry is unbroken, that the Hamiltonian $H^{(2)}$ has the same spectrum of eigenvalues as $H^{(1)}$, except for missing the ground-state energy of $H^{(1)}$:

$$E_n^{(2)} = E_{n+1}^{(1)}. \tag{5}$$

Also, the eigenfunctions of the Hamiltonian $H^{(2)}$ are related to those of $H^{(1)}$ by

$$\psi_n^{(2)}(x) = \frac{A}{\sqrt{E_{n+1}^{(1)}}}\psi_{n+1}^{(1)}(x). \tag{6}$$

Consequently, we can reconstruct all the eigenfunctions of $H^{(1)}$ from those of $H^{(2)}$ except for the ground state

$$\psi_{n+1}^{(1)}(x) = \frac{A^\dagger}{\sqrt{E_n^{(2)}}}\psi_n^{(2)}(x). \tag{7}$$

It is worth noting that the superpotential $W(x)$ is related to the ground state wave function $\psi_0^{(1)}(x)$ by

$$W(x) = -\frac{\hbar}{\sqrt{2m}}\frac{d}{dx}\ln(\psi_0^{(1)}(x)). \tag{8}$$

Using Darboux procedure, one can construct a one-parameter family of strictly isospectral potentials $\widehat{V}^{(1)}(\lambda;x)$, all having the same eigenvalues, to a given initial potential $V^{(1)}(x)$ having at least one bound state. By introducing the function

$$I(x) = \int_{-\infty}^{x} \left[\psi_0^{(1)}(x')\right]^2 dx', \tag{9}$$

the isospectral potentials $\widehat{V}^{(1)}(\lambda\,;x)$ are obtained by the following formula:

$$\widehat{V}^{(1)}(\lambda\,;x) = V^{(1)}(x) - \frac{\hbar^2}{m}\frac{d^2}{dx^2}\ln\left(\frac{1}{\lambda} + \frac{\sqrt{2m}}{\hbar}I(x)\right), \tag{10}$$

where the second term is an anharmonic term that encodes the nonlinear features of these oscillators. Note that we denote the parameter of the isospectral family by $1/\lambda$ instead of λ, as used in literature, in order to better track graphically the asymptotic behavior of our potentials.[63]

These potentials have been used to construct explicit solutions of nonlinear evolution equations[56] and have been used to calculate resonances in a three-dimensional finite square well.[64] The eigenvalues of $\widehat{H}^{(1)}(\lambda\,;x)$ and $H^{(1)}$ are the same. The eigenstates of $\widehat{H}^{(1)}(\lambda\,;x)$ are unitary transforms of those of $H^{(1)}$. The ground state wave functions $\phi_0(x;\lambda)$ may be written in terms of $\psi_0^{(1)}(x)$, the ground state eigenstate of the original Hamiltonian $H^{(1)}(x)$, as follows:

$$\phi_0(x;\lambda) = \frac{\sqrt{1+\lambda\frac{\sqrt{2m}}{\hbar}}}{1+\lambda I(x)\frac{\sqrt{2m}}{\hbar}}\,\psi_0^{(1)}(x), \tag{11}$$

whereas the excited eigenstates of the isospectral Hamiltonians $\widehat{H}^{(1)}(\lambda\,;x)$ are given in terms of both, the excited eigenstates of the states original Hamiltonian $H^{(1)}(x)$

and their corresponding eigenvalues, by the expression

$$\phi_{n+1}(x;\lambda) = \left[1 + \frac{1}{E^{(1)}_{n+1}}\left(\frac{I'(x)}{\frac{1}{\lambda} + \frac{\sqrt{2m}}{\hbar}I(x)}\right) \times \left(\frac{\hbar}{\sqrt{2m}}\frac{d}{dx} + W(x)\right)\right]\psi^{(1)}_{n+1}(x).$$

It should be noted that the eigenfunctions $\phi_n(x;\lambda)$ are square-integrable if and only if $\lambda > -\frac{\hbar}{\sqrt{2m}}$. This is the case we are going to consider in this work.

2.2. *Quantification of nonG*

The nonG of a CV quantum state ρ may be quantified in terms of the statistical distinguishability of the state from a reference Gaussian state ρ_G, chosen to have the same first-moment vector $E[\rho_G]$ and the same covariance matrix $\sigma[\rho_G]$ of ρ (see Appendix A). In particular, the distinguishability is quantified using the quantum relative entropy

$$\delta[\rho] = S(\rho \,\|\, \rho_G) = S(\rho_G) - S(\rho), \tag{12}$$

where $S(\rho) = -\mathrm{Tr}[\rho \log \rho]$ is the Von-Neumann entropy of ρ and for a single-mode Gaussian states

$$S(\rho_G) = h\left(\sqrt{\det\, \sigma[\rho]}\right), \tag{13}$$

where $h(x)$ is a function given by

$$h(t) = \left(t + \frac{1}{2}\right)\ln\left(t + \frac{1}{2}\right) + \left(t - \frac{1}{2}\right)\ln\left(t - \frac{1}{2}\right). \tag{14}$$

Overall, we have the nonG $\delta[\rho]$ of a CV quantum state ρ and may be expressed as

$$\delta[\rho] = h\left(\sqrt{\det\, \sigma[\rho]}\right) - S(\rho). \tag{15}$$

2.3. *NonC measures*

Nonclassical states are conventionally defined as those that cannot be expressed as a statistical mixture of coherent states. This definition is grounded in physical principles and encompasses phenomena that may or may not be observable in experiments. However, in quantum information processing, other characteristics beyond nonC can be crucial for achieving quantum advantage. This has led to the development of more restrictive notions of nonC, tailored to specific applications.[65–78] Evaluating quantum states across these various criteria is essential to assess their potential use in quantum technology. Although it is regrettable that all these measures are referred to as nonC measures, this reflects the current state of the literature, and we will not introduce new terminology here.

In this work, we aim to provide a realistic qualitative and quantitative characterization of both the ground states and the equilibrium states of SHO isospectral potentials. To achieve this, we employ various measures and criteria for nonC, including those based on quadrature squeezing and photon number squeezing, which serve as necessary but not sufficient conditions for fully establishing the non-classical nature of a quantum state. Additionally, we utilize quantitative measures such as the negativity of the Wigner function and the QCS to further refine our analysis.

2.3.1. *Quadrature and photon number squeezing*

Coherent states are minimum uncertainty states, i.e. with uncertainties that are equal for position X and momentum P operators. Similarly squeezed states are minimum uncertainty states but they exhibit less uncertainty in one quadrature and increased fluctuations in the other one. They are non-classical states since this is not compatible with being a mixture of coherent states. For any quantum state, the pair of canonical operators (X, P) obey the Heisenberg uncertainty relation:

$$\Delta X^2 \Delta P^2 \geq \frac{\hbar^2}{4}, \tag{16}$$

where $\Delta X^2 = \langle X^2 \rangle - \langle X \rangle^2$ and $\Delta P^2 = \langle P^2 \rangle - \langle P \rangle^2$ are the variances of the position $\widehat{X}$ and momentum $\widehat{P}$ operators, respectively. Also, the shot noise variance is expressed by the quantity $\dfrac{\hbar}{2}$. The state is said to be squeezed if the variance according to a quadrature is compressed (less than $\hbar/2$). Once we get this squeezing signature, we can say that our state has non-classical features since squeezing implies the singularity of the P-function. Squeezing is thus a sufficient condition for nonC (but not necessary).[79]

Similarly, one speaks of photon number squeezing for those states which satisfy the relation $(\Delta\widehat{n})^2 < \langle \widehat{n} \rangle$ where $\widehat{n} = n|n\rangle\langle n|$ is the photon number operator. This is usually quantified by means of the Fano factor

$$\mathcal{F}[\rho] = \frac{(\Delta\hat{n})^2}{\langle \hat{n} \rangle} = \frac{\langle \hat{n}^2 \rangle - \langle \hat{n} \rangle^2}{\langle \hat{n} \rangle}. \tag{17}$$

If $\mathcal{F}[\rho] < 1$, the photon number distribution is sub-Poissonian and the state is non-classical since this condition is incompatible with having a positive Glauber P-function. Photon number squeezing is a sufficient condition for nonC but it is not a necessary one.

2.3.2. *Wigner negativity*

A celebrated phase-space description of nonC in single mode quantum oscillators is the volume occupied by the negative part of the Wigner function. Since the Wigner function $W(x, p)$ of a quantum state ρ

$$W(x, p) = \frac{1}{\pi\hbar} \int_{-\infty}^{+\infty} \langle x + y|\rho|x - y \rangle e^{-\frac{2ipy}{\hbar}} dy \tag{18}$$

is a normalized (not positive-definite) quasi-probability distribution in the phase space, the Wigner nonC may be written as

$$\nu[\rho] = \left(\iint dx\, dp\, |W(x,p)| \right) - 1. \tag{19}$$

2.3.3. *Quadrature coherence scale (QCS)*

The term *coherences* usually denote the off-diagonal elements $\rho_{aa'} = \langle a|\rho|a'\rangle$ of the density matrix in the eigenbasis of a given observable A. To assess the overall coherence of the state one may introduce the A-coherence scale (squared) of ρ via

$$\mathcal{C}_A^2(\rho) = \frac{1}{\mathcal{P}}\mathrm{Tr}[\rho, A][A, \rho] = \frac{1}{\mathcal{P}} \int (a-a')^2 |\rho(a,a')|^2 da da^{'}, \tag{20}$$

where $\mathcal{P}[\rho] = \mathrm{Tr}[\rho^2]$ is the purity of the state ρ. For a CV system, characterized by the pair of conjugate quadratures (X, P), the QCS is given by

$$\mathcal{C}^2(\rho) = \frac{1}{2}[\mathcal{C}_X^2(\rho) + \mathcal{C}_P^2(\rho)] \tag{21}$$

and quantifies how far from the diagonal the off-diagonal coherences of all quadratures (X, P) lie. A large $\mathcal{C}(\rho)$ implies that for the pair (X, P), at least one has a large coherence scale. When the QCS is small, i.e. $\mathcal{C}(\rho) \leq 1$, the states are close to classical states, whereas for a large QCS, i.e. $\mathcal{C}(\rho) \gg 1$, the states are strongly non-classical, and very sensitive to environmental decoherence.

2.4. *Local quantum parameter estimation*

Many quantities of interest in quantum physics are not accessible by direct measurements because they do not correspond to quantum observables. One can cite temperature, optical phase, and the parameter λ characterizing a family of isospectral potentials. To resolve this issue and assign these quantities a value, we have recourse to indirect measurements within the QET which provides tools to infer the value of an unknown parameter with the optimal possible precision in the quantum limit by finding the best measurements and the best states to achieve this task. In a classical estimation problem, we look for an estimator defined as a function of a finite set of empirical data $\{x_1, x_2, \ldots, x_m\}$ to the set of possible values of the parameter $\hat{\lambda} = \hat{\lambda}(x_1, x_2, \ldots, x_m)$. An unbiased estimator is said to be optimal if it saturates the so-called Cramér–Rao bound (CRB)

$$\mathrm{Var}(\hat{\lambda}) \geq \frac{1}{MF(\lambda)}, \tag{22}$$

which establishes a lower bound on the variance $\mathrm{Var}(\hat{\lambda}) = E_\lambda[(\hat{\lambda}(x) - \lambda)^2]$ of any estimator, M is the number of times the measurement is repeated, and $F(\lambda)$ is the Fisher information (FI):

$$F(\lambda) = \int dx \frac{1}{p(x\,|\,\lambda)} \left(\frac{\partial p(x\,|\,\lambda)}{\partial \lambda} \right)^2, \tag{23}$$

where $p(x \mid \lambda)$ denotes the conditional probability of obtaining the measurement outcome value x when the parameter has the value λ. The FI $F(\lambda)$ can be viewed as a measure of the amount of information carried $p(x \mid \lambda)$ with respect to λ. In quantum mechanics, the conditional probability $p(x \mid \lambda)$ is given by the Born rule $p(x \mid \lambda) = \mathrm{Tr}[\rho_\lambda \hat{\Pi}_x]$, where ρ_λ belongs to a family of quantum states $\{\rho_\lambda\}$ depending on the parameter λ, and forming the quantum statistical model under investigation. $\hat{\Pi}_x$ is an element of the positive operator-valued measure (POVM) representing the measurement with the requirement $\sum_x \hat{\Pi}_x = 1$. Then, FI takes the following form:

$$F(\lambda) = \int dx \frac{(\partial_\lambda \mathrm{Tr}[\rho_\lambda \hat{\Pi}_x])^2}{\mathrm{Tr}[\rho_\lambda \hat{\Pi}_x]}. \tag{24}$$

By introducing the Hermitian operator L_λ, known as the symmetric logarithmic derivative (SLD), which is the solution of the equation $\partial_\lambda \rho_\lambda = \frac{1}{2}(L_\lambda \rho_\lambda + \rho_\lambda L_\lambda)$ one shows that FI can be maximized over all possible generalized measures POVMs by the so-called QFI $H(\lambda)$:

$$H(\lambda) = \mathrm{Tr}[\rho_\lambda L_\lambda^2] \geq F(\lambda), \tag{25}$$

this leads straightforwardly to the definition of the quantum CRB (QCRB)

$$\mathrm{Var}(\widehat{\lambda}) \geq \frac{1}{M\, H(\lambda)} \tag{26}$$

we notice that the QFI depends only on the quantum state ρ_λ, and determines the ultimate bound to precision of any estimation strategy for λ.

By writing the quantum state ρ_λ in its eigenbasis $\rho_\lambda = \sum_n \rho_n(\lambda)|\psi_n(\lambda)\rangle\langle\psi_n(\lambda)|$, where $|\psi_n(\lambda)\rangle$ is an eigenvectors of ρ_λ and $\rho_n(\lambda)$ the corresponding eigenvalue, we then obtain an explicit expression of the QFI given by

$$\begin{aligned} H(\lambda) = {} & \sum_n \frac{(\partial_\lambda \rho_n(\lambda))^2}{\rho_n(\lambda)} \\ & + 2\sum_{n\neq m} \frac{(\rho_n(\lambda) - \rho_m(\lambda))^2}{\rho_n(\lambda) + \rho_m(\lambda)} |\langle\psi_m(\lambda)|\partial_\lambda \psi_n(\lambda)\rangle|^2. \end{aligned} \tag{27}$$

The first term represents the classical FI of the probability distribution $\{p_k\}$, whereas the second term contains the truly quantum contribution to the information accessible to a quantum system. For a generic family of pure states $\rho_\lambda = |\psi(\lambda)\rangle\langle\psi(\lambda)|$, the QFI reduces to the following form:

$$H(\lambda) = 4[\langle\partial_\lambda \psi(\lambda)|\partial_\lambda \psi(\lambda)\rangle + (\langle\partial_\lambda \psi(\lambda)|\psi(\lambda)\rangle)^2]. \tag{28}$$

Note that in a given quantum estimation problem, a quantum measurement is optimal if the condition $F(\lambda) = H(\lambda)$ is met. An estimator is said to be efficient if the corresponding variance saturates the quantum Cramér–Rao inequality. For several relevant quantities in CV quantum information, optimal estimation may be indeed achieved, including entanglement,[80,81] discord,[82,83] loss/dissipation,[84,85] and temperature itself.[86]

3. Isospectral Potentials of the SHO

In this section, we discuss the properties of the supersymmetric isospectral potentials to the harmonic oscillator, which will be employed throughout this paper. We first consider the one-dimensional SHO defined by its position-dependent potential:

$$V^{(1)}(x) = \frac{1}{2}(x^2 - 1), \tag{29}$$

where we adopted the units $\hbar = \omega = m = 1$. In this case the ground state energy is shifted to zero, therefore the energy spectrum is given by $E_n^{(1)} = n$ with $n \geq 0$ and the corresponding normalized wave functions may be written in terms of the Hermite polynomials $H_n(x)$ as

$$\psi_n^{(1)}(x) = \frac{e^{-\frac{x^2}{2}} H_n(x)}{\sqrt[4]{\pi}\sqrt{2^n n!}} \tag{30}$$

$$|n\rangle = \int dx\, \psi_n^{(1)}(x)\, |x\rangle. \tag{31}$$

Within the techniques of SUSY-QM mentioned earlier in Sec. 2.1 and using the expression (9), one obtains the function $I(x)$ in terms of error function $\mathrm{Erf}(x)$:

$$I(x) = \frac{1}{2}[1 + \mathrm{Erf}(x)]. \tag{32}$$

Then, using Eqs. (10), (29) and (32), the one-parameter family of isospectral potentials $\widehat{V}^{(1)}(\lambda\,; x)$ are given by

$$\widehat{V}^{(1)}(\lambda\,; x) = \frac{1}{2}\left(-1 + x^2 + \frac{4\lambda^2 e^{-2x^2}}{\pi[1 + \sqrt{2}\lambda I(x)]^2} + \sqrt{\frac{2}{\pi}}\frac{4\lambda e^{-x^2} x}{1 + \sqrt{2}\lambda I(x)}\right). \tag{33}$$

In the top panel of Fig. 1, we show the isospectral potentials $\widehat{V}^{(1)}(\lambda\,; x)$ as a function of the position coordinate x for three different values of λ. We can see that when λ increases, the form of $\widehat{V}^{(1)}(\lambda\,; x)$ starts developing a local minimum, which becomes deeper and narrower as well as $\lambda \to +\infty$, whereas for $\lambda \to 0$ one gets back the SHO potential, which itself is a member of the isospectral family. As a consequence, the nonlinearity of such oscillators is characterized by the deformation parameter λ and for $\lambda > -\frac{1}{\sqrt{2}}$ the isospectral deformed potentials $\widehat{V}^{(1)}(\lambda\,; x)$ has no singularities. For small values of λ and close to the origin of the real axis, we may write

$$\widehat{V}^{(1)}(\lambda\,; x) = \frac{1}{2}(x^2 - 1) + 2\sqrt{\frac{2}{\pi}}\lambda(x - x^3) + O(x^4),$$

which intuitively explains the presence of a *displaced* minimum, due to the additional linear term, and of the *distortion*, due to the nonlinear cubic terms, in the isospectral deformed potentials.

The ground state of these isospectral oscillators is detached from the rest of the eigenstates and it corresponds to a bound state with zero energy $\widehat{E}_0^{(1)} = 0$. Note that the ground states become more localized and develop larger peaks for larger

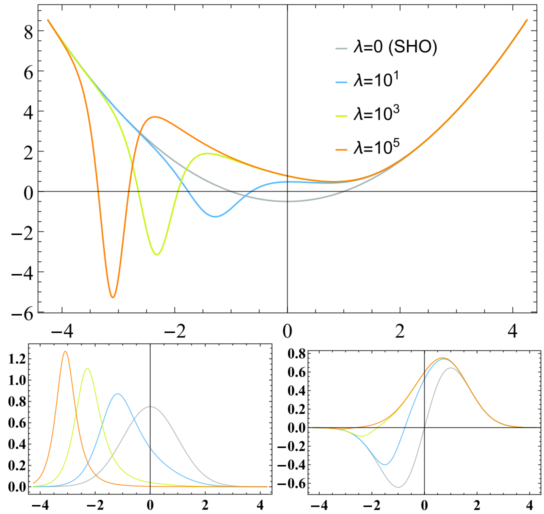

Fig. 1. In the top panel, we show the isospectral SHO potentials $\widehat{V}^{(1)}(\lambda\,;x)$ for $\lambda = 0$ (gray), $\lambda = 10$ (blue), $\lambda = 10^3$ (green), $\lambda = 10^5$ (orange). In the lower left panel, we show the wave functions of the ground state $\phi_0(x;\lambda)$ and, in the lower right panel, those of the first excited state $\phi_1(x;\lambda)$. The color code is the same of the above panel.

values of the deformation parameter λ. Using Eq. (11), the ground state normalized wave function can be obtained as follows:

$$\phi_0(x;\lambda) = \frac{e^{-\frac{1}{2}x^2}}{\pi^{\frac{1}{4}}} \frac{\sqrt{1+\sqrt{2}\lambda}}{1+\sqrt{2}\lambda I(x)}. \tag{34}$$

The behavior of $\phi_0(x;\lambda)$ for some values of λ is shown in the upper-right panel of Fig. 1. For small values of the deformation parameter, we have

$$\phi_0(x;\lambda) = \frac{e^{-\frac{1}{2}x^2}}{\pi^{\frac{1}{4}}} \left[1 - \frac{\lambda}{\sqrt{2}}\,\mathrm{Erf}(x)\right]. \tag{35}$$

Besides, the excited eigenstates are given by

$$\begin{aligned}\phi_{n+1}(x;\lambda) = {}& \frac{2^{-\frac{n}{2}-1}e^{-\frac{3}{2}x^2}}{\pi^{3/4}[1+\sqrt{2}\lambda I(x)]\sqrt{(n+1)!}} \quad n = 0, 1, \ldots \\ & \times \left[\sqrt{\pi}e^{x^2}(2\lambda I(x)+\sqrt{2})H_{n+1}(x) + 2\lambda H_n(x)\right].\end{aligned} \tag{36}$$

$$|\phi_n\rangle = \int dx\, \phi_n(x;\lambda)\, |x\rangle. \tag{37}$$

The first-excited state wave functions are shown in the lower-right panel of Fig. 1, for some values of λ.

4. NonG and nonC of Stationary States

This section is devoted to the study of the properties of the ground and thermal states of the isospectral SHO. Our analysis begins by evaluating their nonG and we investigate their nonC.

4.1. *Ground states*

We start by analyzing the one parameter family of ground states

$$\rho_\lambda = |\phi_0\rangle\langle\phi_0|. \tag{38}$$

The ground state is a pure state, hence its Von Neumann entropy is equal to zero $S(\rho_\lambda) = 0$, therefore the nonG measure (15) reduces to the following form:

$$\delta[\rho_\lambda] = h\left(\sqrt{\det\,\sigma[\rho_\lambda]}\right). \tag{39}$$

For this, the covariance matrix $\sigma[\rho_\lambda]$ is in a diagonal form, where diagonal elements are the variances of canonical operators $\sigma_{11} = \Delta X^2$, $\sigma_{22} = \Delta P^2$. The expectation values and hence the variances can be calculated as in Appendix A.

After looking at the shape of the isospectral ground states in Fig. 1 one would expect that the nonG vanishes for $\lambda \to 0$ and increases with λ. Indeed, this intuitive behavior is captured by a numerical evaluation of $\delta[\rho_\lambda]$ and the corresponding results are reported in Fig. 2.

The nonG increases monotonically (roughly $\propto \lambda^2$) for lower values of the deformation parameter and grows to reach a maximum value $\delta[\rho_\lambda] \simeq 0.26$ for $\lambda \simeq 71$ and then, for larger values of λ, it starts to slowly decrease. This does not seem to have an intuitive explanation, and in order to better capture the nonlinear features of the deformed potentials we will also look, in the next section, at the non-Gaussian properties of thermal states, which account for the whole spectrum of eigenstates.

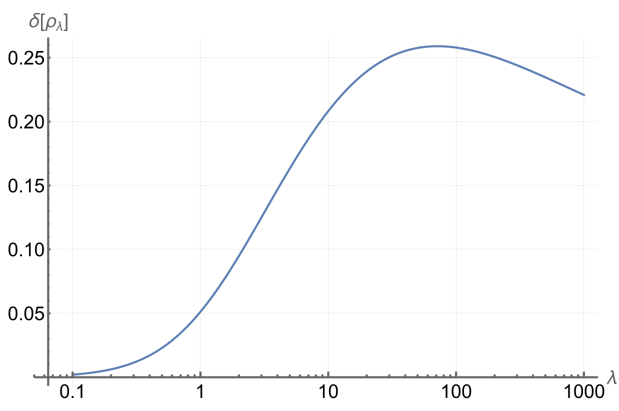

Fig. 2. QRE-based nonG $\delta[\rho_\lambda]$ for the isospectral ground states ρ_λ as a function of the deformation parameter λ.

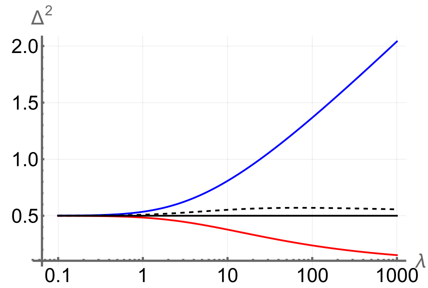

Fig. 3. The variances ΔX^2 (red) and ΔP^2 (blue) for the isospectral ground states ρ_λ as a function of the deformation parameter λ. The solid black line is the shot noise limit $\Delta X^2 = \frac{1}{2}$ and the dashed line denotes the uncertainty product $\Delta X \Delta P$, showing that the isospectral ground state is no longer a minimum uncertainty state.

We conclude that the SUSY procedure has successfully generated an isospectral potentials with eigenstates having the desired non-Gaussian features.

The ground state is also a nonclassical state, as it may be shown by evaluating the variances of the quadrature operators X and P. In particular, the ground state ρ_λ exhibits squeezing, see Fig. 3, in the position quadrature (red line) for any value of the deformation parameter. For $\lambda \to 0$, both variances go back to the shot noise limit (black line). Note that the ground states of the isospectral potentials are no longer minimum uncertainty states (the dashed line denotes the uncertainty product). At variance with quadrature squeezing, the isospectral ground states exhibit photon number squeezing only for large values of the deformation parameter. As it is apparent from the left upper panel of Fig. 4, the Fano factor is larger than

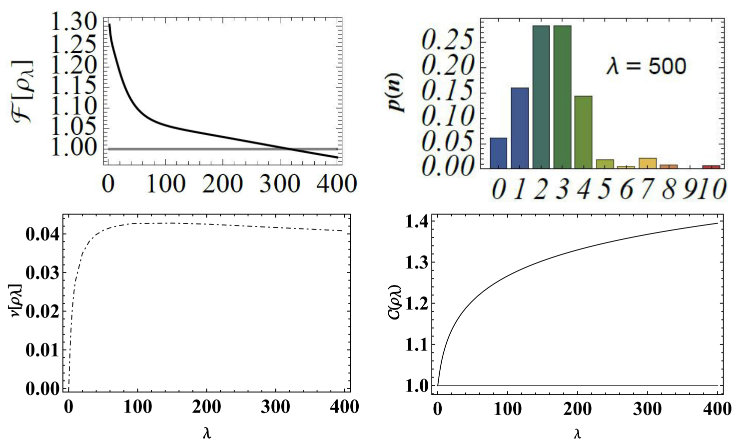

Fig. 4. (Top left): Fano factor $\mathcal{F}[\rho_\lambda]$ for the states ρ_λ as a function of the parameter λ. (Top right): The inset displays the photon number distribution $p(n)$ for the ground state ρ_λ, with $\lambda = 500$. (Bottom left): Wigner negativity $\nu[\rho_\lambda]$ for the isospectral ground states ρ_λ as a function of the deformation parameter λ. (Bottom right): QCS $\mathcal{C}(\rho_\lambda)$ for the states ρ_λ as a function of the parameter λ.

one for $\lambda \leq 315$ and we have a subPoissonian distribution only for larger values of λ. An example of photon distribution is shown in the upper right panel of the same figure.

Finally, in order to quantify the non-classicality of the ground states family, we have numerically evaluate both the Wigner negativity function (19) and the quadrature scale variance (21). The results are reported in the lower panels of Fig. 4, respectively. Note that for pure states, the QCS reduces to the so-called total noise

$$\mathcal{C}^2(\rho_\lambda) = \Delta X^2 + \Delta P^2. \tag{40}$$

Looking at Fig. 4, we see that W-nonclassicality measure $\nu[\rho_\lambda]$, in the left lower panel, shows a behavior analogue to that of the non-Gaussianity measure $\delta[\rho_\lambda]$ in Fig. 2, whereas for the QCS, in the right panel, we can observe that it increases continuously with λ and for $\lambda \to 0$ it reaches its minimal value $\mathcal{C}(\rho) = 1$ corresponding to coherent states with Poissonian profile.

4.2. *Thermal states*

Up to now we have handled just with ground states, i.e. we have assumed the system at zero temperature. In order to analyze more realistic situations, we now consider Gibbs state, i.e. states at thermal equilibrium at temperature T, and analyze how the non-Gaussian and non-classical properties changes as a function of temperature.

The one parameter family of single-mode deformed thermal states ρ_λ^{th} is made of mixtures of the eigenstates with Gibbs weights. In formula

$$\rho_\lambda^{\text{th}} = \sum_{k=0}^{\infty} p_k(T) |\phi_k\rangle\langle\phi_k|, \tag{41}$$

where

$$p_k(T) = \frac{1}{Z} e^{-k/T} \tag{42}$$

the Boltzmann constant has been set to $k_B = 1$ and Z denotes the partition function

$$Z = \sum_{n=0}^{\infty} e^{-n/T} = \frac{e^{1/T}}{e^{1/T} - 1}. \tag{43}$$

In the above formulas, we have already used the isospectrality of all the potentials.

To appreciate the difference between the ground states and the thermal ones, in the following plots we also display the ground states value. The Von Neumann entropy of the states ρ_λ^{th} can be expressed as

$$S(\rho_\lambda^{\text{th}}) = -\sum_{k=0}^{\infty} p_k(T) \log p_k(T) \tag{44}$$

hence, the QRE nonG measure (15) for the thermal states ρ_λ^{th} is given as follows

$$\delta[\rho_\lambda^{\text{th}}] = h\left(\sqrt{\det \sigma \left[\rho_\lambda^{\text{th}}\right]}\right) + \sum_{k=0}^{\infty} p_k(T) \log p_k(T). \tag{45}$$

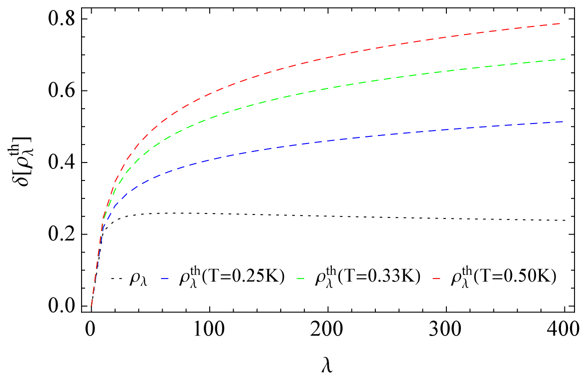

Fig. 5. QRE-based nonG $\delta[\rho_\lambda^{\mathrm{th}}]$ as a function of the deformation parameter λ for isospectral thermal states $\rho_\lambda^{\mathrm{th}}$ with $T = 0.25K$ (dashed blue), $T = 0.33K$ (dashed green) and $T = 0.50K$ (dashed red). The dotted black line refers to the nonG of ground states family $\delta[\rho_\lambda]$.

In Fig. 5, we show the numerically evaluated QRE nonG measure for three thermal states $\rho_\lambda^{\mathrm{th}}$ with different values of temperature T (see the legend). For comparison, we have also plotted the nonG of the ground state. For small values $\lambda \lesssim 10$, the QRE nonG measure increases monotonically with λ, exhibiting the same behavior for all considered families of thermal states $\rho_\lambda^{\mathrm{th}}$. For larger values $\lambda > 10$, the nonG continues to increase, though less rapidly, and is larger for larger T. This means that temperature enhances the nonlinearity-induced nonGaussianity. The same, however, does not happen for non-classicality, as we discuss in the following.

From the evaluation of the variance $(\Delta X)^2$ for the three families of thermal states (see the upper left panel of Fig. 6), we can observe that thermal states exhibit squeezing for low temperatures $T < 0.33K$, while increasing temperature makes it to surpass the shot noise limit. From the upper right panel of the same figure, we see that for low temperatures $T < 0.33K$, the Fano factor decreases as the deformation parameter λ increases. Considering the family of thermal states with $T = 0.25K$ (dashed blue) we note a sub-Poissonian distributions, $\mathcal{F}[\rho_\lambda^{\mathrm{th}}] < 1$ for $\lambda > 900$. On the other hand, for higher temperatures $T \geq 0.33K$ the Fano factor increases with temperature. Finally, to further characterize and quantify the non-classicality of the families of thermal states, we have numerically evaluated both the Wigner negativity function (19) and the QCS (21). Results are reported in the lower panels of Fig. 6. Note that QCS is calculated via the formula

$$\mathcal{C}^2(\rho^{\mathrm{th}}) = \mathcal{P}^2(\Delta X^2 + \Delta P^2), \tag{46}$$

where $\mathcal{P}$ is the purity. For these measures of non-classicality in thermal states, we see a decrease for increasing temperature. Besides, at fixed value of T, they are affected by the deformation parameter λ. In particular, (see left panel) for low values of λ the Wigner negativity increases monotonically as a function of λ until reach a maximum, and then decreases slowly going to an asymptotic value. In the right

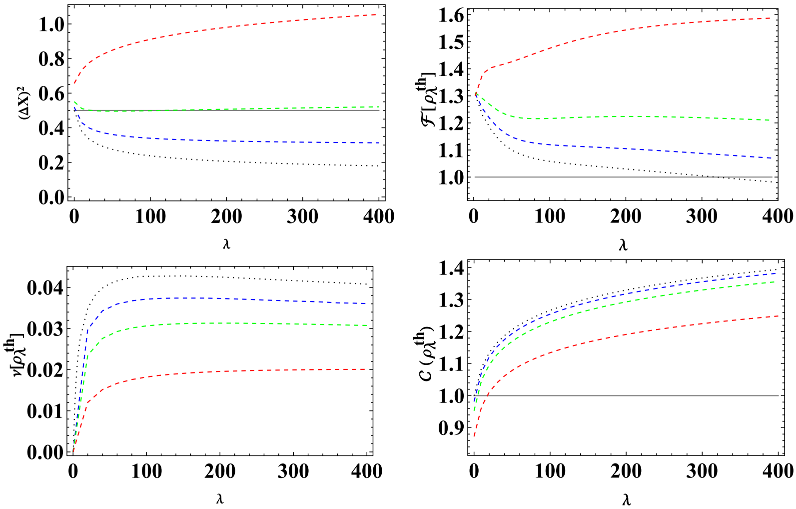

Fig. 6. (Top left): Squeezing quadrature $(\Delta X)^2$ for the isospectral thermal states $\rho_\lambda^{\mathrm{th}}$ as a function of the deformation parameter λ for different value of the temperature. (Top right): Fano factor $\mathcal{F}\left[\rho_\lambda^{\mathrm{th}}\right]$. (Bottom left): Wigner negativity $\nu[\rho_\lambda]$. (Bottom right): QCS $\mathcal{C}(\rho_\lambda^{\mathrm{th}})$. In all plots, the red dotted line denotes the curve for $T = 0.5K$, green is for $T = 0.33K$ and blue for $T = 0.25K$. The black dotted lines correspond to the measures of the ground states ρ_λ, that is to the limit $T \to 0$.

panel, we observe that QCS increases continuously with λ, whereas it approaches the limit $\mathcal{C}(\rho) = 1$ of "*quadrature quasi-incoherent states*" as $\lambda \to 0$.

5. Characterization of the SHO Isospectral Potentials

Here we present some results about the characterization of isospectral oscillators, focusing on the ultimate bounds on the precision in estimating the deformation parameter λ. In particular, we address optimal measurement protocols and evaluate the corresponding QFI.

In the simplest configuration, the precision in the estimation of the deformation parameter λ is quantified by the QFI $H(\lambda)$ for the isospectral ground states ρ_λ, which itself may be evaluated using Eq. (28), arriving at

$$H(\lambda) = \frac{2}{3}\frac{1}{(1+\sqrt{2}\lambda)^2}. \tag{47}$$

Remarkably, the quantum CRB (QCRB) is achieved by position measurements, i.e. by measuring the position operator X of the oscillator, we have $F(\lambda) = H(\lambda)$. The QFI is a decreasing function of λ and vanishes for great values of λ, thus indicating that any estimator $\widehat{\lambda}$ of the deformation parameter λ becomes less and less precise for large λ. The QFI, however, decreases only quadratically with the parameter and therefore the signal-to-noise ratio scales as $\lambda^2/\mathrm{Var}\lambda \to \frac{1}{3} - O(1/\lambda)$, i.e. it remains finite even for $\lambda \to \infty$. For thermal states, the QFI for the parameter

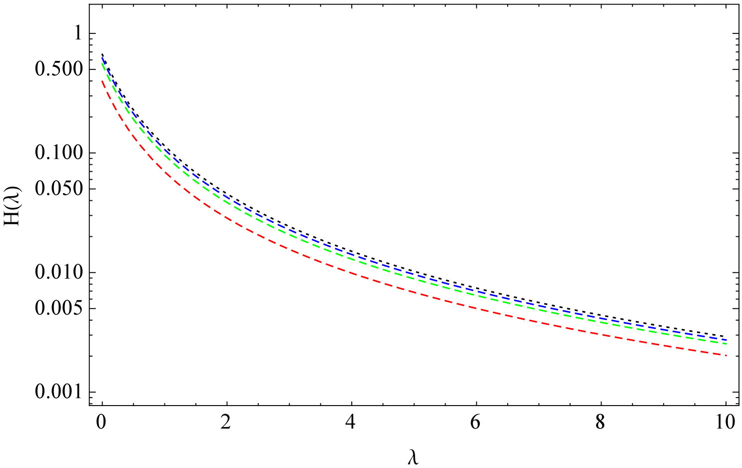

Fig. 7. QFI for isospectral SHO thermal states $\rho_\lambda^{\rm th}$ as a function of the deformation parameter λ. The dashed curves are for increasing values of T (shown in the legend) from top to bottom. The dotted line at the top is the ground state QFI.

λ at temperature T is given by

$$H(\lambda;T) = 2\sum_{n\neq m}\frac{[p_n(T)-p_m(T)]^2}{p_n(T)+p_m(T)}|\langle\phi_m|\partial_\lambda\phi_n\rangle|^2. \tag{48}$$

In Fig. 7, we show the behavior of the QFI $H(\lambda;T)$ at fixed temperatures as a function of λ. The QFI shows the same qualitative behavior as that for ground states (Black dots), i.e. it decreases with the deformation parameter λ. At fixed λ, the QFI slightly decreases with temperature. Also in this case, the FI of position measurement equals the QFI. In other words, position data provide us with all the maximum available information about the deformation parameter of the isospectral potentials.

6. Conclusion

Nonlinear oscillators have attracted interest in different fields, as they play a relevant role for fundamental and practical purposes. In particular, they have recently received attention as a possible resource for quantum information processing. In this paper, we have focused on SUSY potentials isospectral to the SHO and shown that the ground state of the λ-isospectral potentials is non-Gaussian for all positive values of λ with the non-Gaussianity persisting in thermal states and increasing with temperature. The states are also non-classical as confirmed by the emergence of squeezing of the ground state and also photon-number squeezing for large values of the deformation parameter. Additionally, we have shown that the ground state exhibits Wigner negativity, which increases with the deformation parameters until reaching a maximum and then slowly decreases. Non-classicality is also present in the equilibrium states of the systems up to some threshold temperature.

We have also addressed the characterization of the systems, i.e. the estimation of the deformation parameter and evaluated the QFI. We found for the pure state model the QFI decreases with increasing values of the parameter, and the CRB is saturated by position measurement. The QFI for thermal states exhibits a qualitatively similar behavior with a slight decrease in value at higher temperatures. The QFI decreases for increasing λ and vanishes in the limit $\lambda \to \infty$. The optimal measurement is still the position measurement which saturates the CRB.

In conclusion, our study proves an interesting interplay between SUSYQM and nonlinearity, unveiling the remarkable non-Gaussian and non-classical properties of the eigenstates of λ-isospectral potentials. The persistence of these features in thermal states and their dependence on temperature and the deformation parameter confirm the robustness of these systems for exploring fundamental quantum phenomena. Moreover, we have addressed the bounds to precision in the characterization of systems described by isospectral SUSY potentials, with position measurements emerging as an optimal strategy. Our results deepen our understanding of isospectral potentials and prove they may represent promising platforms for quantum information with CVs, particularly in leveraging their non-classical and non-Gaussian properties. We hope that our results will pave the way for further exploration, e.g. using coherent states of isospectral oscillators,[63] into the practical applications of nonlinearity and SUSY in quantum technologies.

Appendix A. Displacement Vector and Covariance Matrix of a Quantum State

Introducing the real vector of canonical operators $R = (X, P)^T$, the displacement vector $E[\rho]$ and the covariance matrix $\sigma[\rho]$ of a quantum state are given by

$$E[\rho] = (\langle X\rangle, \langle P\rangle)^T, \tag{A.1}$$

$$\sigma[\rho] = \begin{pmatrix} \Delta X^2 & \dfrac{\langle XP\rangle + \langle PX\rangle}{2} - \langle X\rangle\langle P\rangle \\ \dfrac{\langle XP\rangle + \langle PX\rangle}{2} - \langle X\rangle\langle P\rangle & \Delta P^2 \end{pmatrix}. \tag{A.2}$$

For a generic pure state $|\phi\rangle$, we have

$$\langle X\rangle = \langle \phi|X|\phi\rangle = \int_{\mathbb{R}} dx\, x\, |\phi(x)|^2, \tag{A.3}$$

$$\langle P\rangle = \langle \phi|P|\phi\rangle = -i\hbar \int_{\mathbb{R}} dx\, \phi(x)\, \partial_x \phi(x), \tag{A.4}$$

$$\langle X^2\rangle = \langle \phi|X^2|\phi\rangle = \int_{\mathbb{R}} dx\, x^2\, |\phi(x)|^2, \tag{A.5}$$

$$\langle P^2 \rangle = \langle \phi | P^2 | \phi \rangle = -\hbar^2 \int_{\mathbb{R}} dx\, \phi(x)\, \partial_x^2 \phi(x), \tag{A.6}$$

$$\langle XP \rangle = \langle \phi | XP | \phi \rangle = -i\hbar \int_{\mathbb{R}} dx\, \phi(x)\, x\, \partial_x \phi(x), \tag{A.7}$$

$$\langle PX \rangle = \langle \phi | PX | \phi \rangle = -i\hbar \int_{\mathbb{R}} dx\, \phi(x)\, \partial_x [x\, \phi(x)]. \tag{A.8}$$

ORCID

Abdelatif Chabane https://orcid.org/0000-0003-0506-2529
Sidali Mohammdi https://orcid.org/0009-0009-8357-6868
Abdelhakim Gharbi https://orcid.org/0000-0003-2995-3238
Matteo G. A. Paris https://orcid.org/0000-0001-7523-7289

References

1. S. L. Braunstein and P. van Loock, *Rev. Mod. Phys.* **77** (2005) 513.
2. U. L. Andersen, G. Leuchs and C. Silberhorn, *Laser Photon. Rev.* **4** (2010) 337.
3. N. J. Cerf, G. Leuchs and E. S. Polzik, *Quantum Information with Continuous Variables of Atoms and Light* (World Scientific, 2007).
4. A. Ferraro, S. Olivares and M. G. A. Paris, *Gaussian States in Continuous Variable Quantum Information* (Bibliopolis, Napoli, 2005).
5. G. Giedke and J. I. Cirac, *Phys. Rev. A* **66** (2002) 032316.
6. C. Navarrete-Benlloch, *An Introduction to the Formalism of Quantum Information with Continuous Variables* (Morgan & Claypool Publishers, 2015).
7. N. Killoran, T. R. Bromley, J. M. Arrazola, M. Schuld, N. Quesada and S. Lloyd, *Phys. Rev. Res.* **1** (2019) 033063.
8. S. Lloyd and S. L. Braunstein, *Phys. Rev. Lett.* **82** (1999) 1784.
9. P. van Loock, *Fortsch. Phys. Prog. Phys.* **50** (2002) 1177.
10. N. C. Menicucci, P. Van Loock, M. Gu, C. Weedbrook, F. T. C. Ralph and M. A. Nielsen, *Phys. Rev. Lett.* **97** (2006) 110501.
11. R. Ukai, J.-I. Yoshikawa, N. Iwata, P. van Loock and A. Furusawa, *Phys. Rev. A* **81** (2010) 032315.
12. S. T. Flammia, N. C. Menicucci and O. Pfister, *J. Phys. B: Atom. Molecul. Opt. Phys.* **42** (2009) 114009.
13. A. Serafini, *Quantum Continuous Variables: A Primer of Theoretical Methods* (CRC Press, 2023).
14. C. Weedbrook, S. Pirandola, R. García-Patrón, N. J. Cerf, T. C. Ralph, J. H. Shapiro and S. Lloyd, *Rev. Mod. Phys.* **84** (2012) 621.
15. P. Jouguet, S. Kunz-Jacques and A. Leverrier, *Phys. Rev. A* **84** (2011) 062317.
16. N. C. Menicucci, *Phys. Rev. Lett.* **112** (2014) 120504.
17. S. L. Braunstein, *Phys. Rev. Lett.* **80** (1998) 4084.
18. R. L. Hudson, *Rep. Math. Phys.* **6** (1974) 249.
19. F. Soto and P. Claverie, *J. Math. Phys.* **24** (1983) 97.
20. S. D. Bartlett, B. C. Sanders, S. L. Braunstein and K. Nemoto, *Phys. Rev. Lett.* **88** (2002) 097904.
21. M. Ohliger, K. Kieling and J. Eisert, *Phys. Rev. A* **82** (2010) 042336.
22. M. Walschaers, *PRX Quantum* **2** (2021) 030204.

23. G. Kitagawa, *J. Amer. Statist. Assoc.* **82** (1987) 1032.
24. K. Mølmer, *Phys. Rev. A* **73** (2006) 063804.
25. S. Olivares, M. G. A. Paris and R. Bonifacio, *Phys. Rev. A* **67** (2003) 032314.
26. H. Adnane, M. Bina, F. Albarelli, A. Gharbi and M. G. A. Paris, *Phys. Rev. A* **99** (2019) 063823.
27. H. Adnane, B. Teklu and M. G. A. Paris, *J. Opt. Soc. Am. B* **36** (2019) 2938.
28. M. G. Genoni and M. G. A. Paris, *Phys. Rev. A* **82** (2010) 052341.
29. S. Takeda, H. Benichi, T. Mizuta, N. Lee, J.-I. Yoshikawa and A. Furusawa, *Phys. Rev. A* **85** (2012) 053824.
30. J. Singh and S. Bose, *Phys. Rev. A* **104** (2021) 052605.
31. L. Hu, M. Al-Amri, Z. Liao and M. Zubairy, *Phys. Rev. A* **102** (2020) 012608.
32. A. Leverrier and P. Grangier, *Phys. Rev. A* **83** (2011) 042312.
33. Y. Guo, W. Ye, H. Zhong and Q. Liao, *Phys. Rev. A* **99** (2019) 032327.
34. P. Huang, G. He, J. Fang and G. Zeng, *Phys. Rev. A* **87** (2013) 012317.
35. J. Niset, J. Fiurášek and N. J. Cerf, *Phys. Rev. Lett.* **102** (2009) 120501.
36. E. Knill, R. Laflamme and G. J. Milburn, *Nature* **409** (2001) 46.
37. G. Adesso, F. Dell'Anno, S. De Siena, F. Illuminati and L. Souza, *Phys. Rev. A* **79** (2009) 040305.
38. K. K. Sabapathy and A. Winter, *Phys. Rev. A* **95** (2017) 062309.
39. N. J. Cerf, O. Krüger, P. Navez, R. F. Werner and M. M. Wolf, *Phys. Rev. Lett.* **95** (2005) 070501.
40. The LIGO Scientific Collab., *Nature Phys.* **7** (2011) 962.
41. J. Aasi *et al.*, *Nature Photon.* **7** (2013) 613.
42. F. Acernese *et al.*, *Phys. Rev. Lett.* **123** (2019) 231108.
43. M. Tse *et al.*, *Phys. Rev. Lett.* **123** (2019) 231107.
44. M. Walschaers, V. Parigi and N. Treps, *PRX Quantum* **1** (2020) 020305.
45. A. Lvovsky, P. Grangier, A. Ourjoumtsev, V. Parigi, M. Sasaki and R. Tualle-Brouri, arXiv:2006.16985.
46. A. Ourjoumtsev, R. Tualle-Brouri, J. Laurat and P. Grangier, *Science* **312** (2006) 83.
47. J. Wenger, R. Tualle-Brouri and P. Grangier, *Phys. Rev. Lett.* **92** (2004) 153601.
48. A. Zavatta, V. Parigi, M. Kim and M. Bellini, *New J. Phys.* **10** (2008) 123006.
49. V. Averchenko, C. Jacquard, V. Thiel, C. Fabre and N. Treps, *New J. Phys.* **18** (2016) 083042.
50. V. Parigi, A. Zavatta, M. Kim and M. Bellini, *Science* **317** (2007) 1890.
51. H. S. Chuong and T. M. Duc, *J. Phys. B*: *Atom. Molecul. Opt. Phys.* **56** (2023) 205401.
52. P. Malpani, K. Thapliyal, N. Alam, A. Pathak, V. Narayanan and S. Banerjee, *Opt. Commun.* **459** (2020) 124964.
53. F. Cooper, A. Khare and U. Sukhatme, *Phys. Rep.* **251** (1995) 267.
54. D. Fernández C, M. Glasser and L. Nieto, *Phys. Lett. A* **240** (1998) 15.
55. W.-Y. Keung, U. P. Sukhatme, Q. Wang and T. D. Imbo, *J. Phys. A*: *Math. Gen.* **22** (1989) L987.
56. A. Khare and U. Sukhatme, *J. Phys. A*: *Math. Gen.* **22** (1989) 2847.
57. O. Steuernagel and A. B. Klimov, *Phys. Lett. A* **392** (2021) 127144.
58. Y. Nasuda and N. Sawado, *Phys. Scr.* **99** (2024) 045212.
59. A. S. Holevo, *Probabilistic and Statistical Aspects of Quantum Theory* (Springer Science & Business Media, 2011).
60. C. W. Helstrom, *J. Statist. Phys.* **1** (1969) 231.
61. M. G. A. Paris, *Int. J. Quantum Inform.* **7** (2009) 125.

62. F. Albarelli, M. Barbieri, M. G. Genoni and I. Gianani, *Phys. Lett. A* **384** (2020) 126311.
63. M. Sanjay Kumar and A. Khare, *Phys. Lett. A* **217** (1996) 73.
64. T. K. Das and B. Chakrabarti, *Phys. Lett. A* **288** (2001) 4.
65. C. T. Lee, *Phys. Rev. A* **44** (1991) R2775.
66. C. T. Lee, *Phys. Rev. A* **45** (1992) 6586.
67. M. G. A. Paris, *Phys. Lett. A* **289** (2001) 167.
68. V. Dodonov, *J. Opt. B*: *Quantum Semiclass. Opt.* **4** (2002) R1.
69. P. Marian, T. A. Marian and H. Scutaru, *Phys. Rev. Lett.* **88** (2002) 153601.
70. V. Dodonov and M. Renó, *Phys. Lett. A* **308** (2003) 249.
71. E. V. Shchukin and W. Vogel, *Phys. Rev. A* **72** (2005) 043808.
72. A. Ferraro and M. G. A. Paris, *Phys. Rev. Lett.* **108** (2012) 260403.
73. R. J. Glauber, *Phys. Rev.* **131** (1963) 2766.
74. A. Kenfack and K. Życzkowski, *J. Opt. B*: *Quantum Semiclass. Opt.* **6** (2004) 396.
75. A. Mari, K. Kieling, B. M. Nielsen, E. Polzik and J. Eisert, *Phys. Rev. Lett.* **106** (2011) 010403.
76. S. De Bievre, D. B. Horoshko, G. Patera and M. I. Kolobov, *Phys. Rev. Lett.* **122** (2019) 080402.
77. A. Hertz and S. De Bievre, *Phys. Rev. Lett.* **124** (2020) 090402.
78. A. Hertz and S. De Bièvre, *Phys. Rev. A* **107** (2023) 043713.
79. G. S. Agarwal, *Quantum Optics* (Cambridge University Press, 2012).
80. M. G. Genoni, P. Giorda and M. G. A. Paris, *Phys. Rev. A* **78** (2008) 032303.
81. G. Brida, I. P. Degiovanni, A. Florio, M. Genovese, P. Giorda, A. Meda, M. G. A. Paris and A. Shurupov, *Phys. Rev. Lett.* **104** (2010) 100501.
82. M. Shi, C. Sun, F. Jiang, X. Yan and J. Du, *Phys. Rev. A* **85** (2012) 064104.
83. S. Virzì, E. Rebufello, A. Avella, F. Piacentini, M. Gramegna, I. Ruo Berchera, I. P. Degiovanni and M. Genovese, *Sci. Rep.* **9** (2019) 3030.
84. A. Monras and M. G. A. Paris, *Phys. Rev. Lett.* **98** (2007) 160401.
85. C. Invernizzi, M. G. A. Paris and S. Pirandola, *Phys. Rev. A* **84** (2011) 022334.
86. M. G. A. Paris, *J. Phys. A*: *Math. Theor.* **49** (2015) 03LT02.